

Article

# Omindirectional Non-Reciprocity via 2D Modulated Radial Sonic Crystals

Davide Enrico Quadrelli , Emanuele Riva , Gabriele Cazzulani  and Francesco Braghin 

Department of Mechanical Engineering, Politecnico di Milano, via La Masa 1, 20156 Milano, Italy; emanuele.riva@polimi.it (E.R.); gabriele.cazzulani@polimi.it (G.C.); francesco.braghin@polimi.it (F.B.)

\* Correspondence: davideenrico.quadrelli@polimi.it

Received: 26 June 2020; Accepted: 14 July 2020; Published: 17 July 2020



**Abstract:** In this paper we report on nonreciprocal wave propagation in a 2D radial sonic crystal with space–time varying properties. We show that a modulation traveling along the radial direction reflects in omni-directional and isotropic nonreciprocal wave propagation between inner and outer shells. The nonreciprocal behavior is verified both analytically and numerically, demonstrating that space–time radial crystals can be employed as one-way emitter or receiver of acoustic or elastic signals.

**Keywords:** nonreciprocity; acoustic diode; radial sonic crystal (RSC); spatiotemporal

## 1. Introduction

Based on the reciprocity principle, wave propagation in linear unmodulated materials occurs with the same dispersion characteristics along opposite directions. Dispersion properties showing lack of mirror symmetry in the wavevector space witness the breaking of such principle, implying directional propagation characteristics. The breaking of reciprocity is considered an interesting topic within the research community and is motivated by numerous applications of technological relevance for different realms of physics, such as mechanical [1–6], acoustic [7–9], and electromagnetic [10] systems. In this context, one dimensional space–time modulations have been successfully conceived to generate filtering bands (or *bandgaps*) occurring at different frequencies for counter propagating waves. Topical examples of space–time modulation have been successfully realized in elastic structures through piezoelectric material with attached negative capacitance shunts [11,12]. Similarly, passive beams with embedded resonators have been used for this purpose, by properly phase shifting consecutive modulation signals, mimicking a plane wave propagation along the beam’s dimension [13–15]. The acoustic counterpart has been studied by Cummer and co-workers [7,16,17] and S. Karkar et al. [8], among others [18,19], demonstrating strong nonreciprocal transmission of acoustic waves. In addition, nonreciprocity in modulated electromagnetic waveguides have been object of research in the last years, with emphasis on Bloch modes conversion [20,21] and stability [22,23].

Recently, 2D space–time varying systems have been employed as a platform to break the reciprocity principle, following the same approach adopted in the monodimensional case [24,25]. The performances of such configuration is mainly limited by two factors: (i) modulations traveling along specific directions lead to modified dispersion for a limited range of propagation angles, which implies strong anisotropy in the nonreciprocal response; (ii) the generation of complete nonreciprocal bandgaps can be problematic for the greater number of supported modes as compared to the monodimensional counterparts.

In the attempt to overcome such limitation, we consider a class of axisymmetric modulations, called radial sonic crystals (RSCs), which have been successfully employed by Torrent and co-workers to induce reciprocal bandgaps in prior studies [26].

In contrast with Ref. [26], we introduce the Plane Wave Expansion Method (PWEM) for the analysis of spatially modulated RSCs. Then, such analysis tool is employed to investigate on the propagation properties of space–time varying media. In this context, the breaking of reciprocity principle is achieved through an RSC in which the modulation embodies a space–time variation of the material properties in the radial direction.

For this configuration, we demonstrate that omnidirectional isotropic nonreciprocity can be achieved for acoustic waves, i.e., there are given frequency bands in which only diverging waves can propagate freely, while the existence of propagating converging ones is forbidden and vice-versa, depending on the direction of propagation of the modulation. The concept is elucidated in Figure 1, showing that wave can propagate when traveling opposite to the modulation, whereas a filtering effect is achieved in case of a concurrent propagation direction. More specifically, we show that RSCs support distinct Bloch modes, each characterized by a different azimuthal symmetry (monopole, dipole, quadrupole, etc.), that propagate along the radial direction and can be isolated through a selective excitation, therefore achieving one-way effects between inner and outer shells.

The article is organized as follows: in Section 2 the PWEM for radial crystals is introduced as the main analysis tool adopted in this manuscript. Section 3 deals with the application of such method in the attempt to compute the wave propagation properties of spatially modulated RSCs, as a preliminary case study for the main discussion of this work. The analytical results are then verified via numerical simulations of the RSC under wide spectrum excitation. The analysis then is focused on space–time varying RSCs, for which the occurrence of the nonreciprocal behavior is verified through the PWEM and by way of numerical simulations of wave propagation under narrowband transient excitation. In this context, we demonstrate that space–time varying RSCs operate as a one-way emitter or receiver of acoustic waves. Concluding remarks are reported in Section 4.

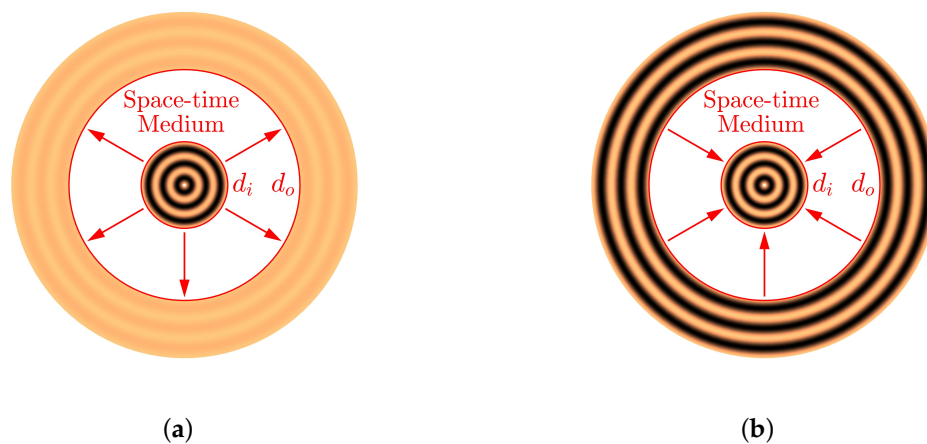


**Figure 1.** Graphical representation of the one-way effect. (a) Waves are allowed to propagate from the inner to the outer shells  $d_i$  and  $d_o$  of the spatiotemporally modulated radial sonic crystal (RSC) (white region in the drawing) when the modulation travels from the outer to the inner shell. (b) Vice-versa, waves are not allowed to reach the outer shell if the modulation travels from the inner to the outer shell.

## 2. Materials and Methods

Following the work presented in Ref. [26], we briefly underline the conditions under which the Bloch theorem can be applied in case axisymmetric variation of material properties in radial direction is considered (the temporal modulation will be introduced in the next section). We hereafter introduce the PWEM to compute the dispersion properties of RSCs. With implied harmonic time dependence and

under the assumption that  $p(r, \theta) = \sum_q p_q(r) e^{iq\theta}$ , the acoustic wave equation for a non homogeneous medium in cylindrical coordinates writes:

$$\left(-B(r) \frac{1}{r} \frac{\partial}{\partial r} r \frac{\partial}{\partial r} \frac{1}{\rho(r)} + \frac{B(r)}{\rho(r)} \frac{q^2}{r^2}\right) p_q = \omega^2 p_q \tag{1}$$

where  $B(r)$  is the bulk modulus of the fluid and  $\rho(r)$  its mass density. The underlying assumption is that the material parameters are constant in the azimuthal direction. The wave equation can be recasted in the following form:

$$\mathcal{H}_q w_q = \omega^2 w_q \tag{2}$$

defining the differential operator

$$\mathcal{H}_q = -B(r) \frac{1}{r} \frac{\partial}{\partial r} r \frac{\partial}{\partial r} \frac{1}{\rho(r)} + \frac{B(r)}{\rho(r)} \frac{q^2}{r^2} \tag{3}$$

For the Bloch theorem to hold,  $\mathcal{H}_q$  should be invariant under the translations defined by  $r \rightarrow r + nd$ , with  $n$  integer and  $d$  the radial lattice constant. As previously shown in Ref. [26], this is only possible if a tensorial mass density is assumed:

$$\left[-\frac{B(r)}{r} \frac{\partial}{\partial r} r \frac{\partial}{\partial r} \frac{1}{\rho_r(r)} + q^2 \frac{B(r)}{r^2 \rho_\theta(r)}\right] p_q(r) = \omega^2 p_q(r) \tag{4}$$

where  $\rho_r(r)$  and  $\rho_\theta(r)$  are introduced as the components of the mass density tensor. Based on the aforementioned arguments, the desired translational invariance can be recovered when the following coefficients in the differential operator are adopted:

$$\begin{aligned} B(r) &= r \sum_n B_n e^{in\kappa_r r} \\ \frac{1}{\rho_r(r)} &= \frac{\sum_n R_n e^{in\kappa_r r}}{r} \\ \frac{1}{\rho_\theta(r)} &= r \sum_n \Theta_n e^{in\kappa_r r} \end{aligned} \tag{5}$$

which allow for the evaluation of the dispersion properties in the  $\omega = \omega(\kappa)$  form to be found upon application of the Bloch theorem. Here  $\kappa_r = 2\pi/d$  and  $n \in [-N, N]$  is the index of the Fourier expansion. As a consequence, Bloch waves are admissible solutions for Equation (4):

$$p_q(r) = \sum_m P_{q,m} e^{i(m\kappa_r + \kappa)r} \tag{6}$$

Upon substitution of Equations (5) and (6) in Equation (4) and exploiting the orthogonality of the exponential functions, an eigenvalue problem can be obtained in the form (see the details in Appendix A):

$$[H(\kappa)] \mathbf{W}_q = \omega^2 \mathbf{W}_q \tag{7}$$

which yields the dispersion relation  $\omega(\kappa)$  of the RSC for Bloch waves traveling along the radial direction  $r$ , while the dependence from  $\theta$  is implicit in the  $q$  value.

Consider now a space–time modulation of the material parameters:

$$\begin{aligned} B(r, t) &= \sum_n B_n e^{in(\kappa_r r - \omega_r t)} \\ \frac{1}{\rho_r(r, t)} &= \frac{\sum_n R_n e^{in(\kappa_r r - \omega_r t)}}{r} \\ \frac{1}{\rho_\theta(r, t)} &= r \sum_n \Theta_n e^{in(\kappa_r r - \omega_r t)} \end{aligned} \quad (8)$$

which corresponds to the space-varying configuration, augmented by a temporal modulation with angular frequency  $\omega_r = 2\pi/T_r$ .  $T_r$  is the temporal period. Bloch-wave solutions take the following form:

$$p_q(r, t) = \sum_m P_{q,m} e^{i[(m\kappa_r + \kappa)r - (m\omega_r + \omega)t]} \quad (9)$$

Similarly to the spatially modulated medium, we exploit the PWEM to get to a quadratic eigenvalue problem (QEP):

$$\omega^2 [M_2] + \omega [M_1] + [M_0(\kappa)] = 0 \quad (10)$$

where the matrices  $[M_2] = [I]$ ,  $[M_1]_{ij} = 2\omega_r i \delta_{ij}$ , and  $[M_0]_{ij} = \omega_r^2 i^2 \delta_{ij} - [H(\kappa)]_{ij}$  are detailed in Appendix B. Equation (10) is used to evaluate the dispersion relation  $\omega(\kappa)$  for given values of  $q$  and hereafter employed to study a specific class of radial space–time modulations.

### 3. Results

#### 3.1. Space-Varying Radial Crystals

Let us consider the material properties illustrated in Figure 2. In the case at hand we assume  $B_n = \Theta_n = \delta_{0n}$  without any loss in generality, where  $\delta_{0n}$  is the symbol of Kronecker, i.e.,  $\rho_r(r, \theta)$  and  $\rho_\theta(r, \theta)$  are constants modulated by  $r$ . In contrast, the radial density  $\rho_r(r, \theta)$  is spatially modulated such that:

$$\sum_n R_n e^{in\kappa_r r} = R_0 [1 + \alpha \cos(\kappa_r r)] \quad (11)$$

with a spatial period  $d = 1$  m, and a dimensionless modulation amplitude  $\alpha = \Delta R/R_0 = 0.4$ , with  $\Delta R = (R_{max} - R_{min})/2$ .  $R(r, \theta) = \sum_n R_n e^{in\kappa_r r}$  is shown in Figure 2a to better highlight the imposed periodicity. The radial density  $\rho_r(r, \theta) = \rho_r(r)$ , azimuthal density  $\rho_\theta(r, \theta) = \rho_\theta(r)$  and the bulk modulus  $B(r, \theta) = B(r)$  are instead represented in Figure 2b–d and are evaluated through Equation (5). We remark that the physical parameters adopted in the manuscript have been arbitrarily set and do not affect the physical behavior of the system, but only have influence on the frequency range under consideration.

Note that different  $q$  values lead to different dispersion branches, corresponding to different azimuthal symmetries. The Bloch diagrams are shown with white dots in Figure 3a–c for  $q = 0, 1, 2$ , and are evaluated through the aforementioned method. In the figure and in the remainder of the manuscript,  $\mu = \kappa d$  is defined as the normalized wavenumber, which implies that the Brillouin zone is limited within the domain  $\mu/\pi \in [-1, 1]$ . The associated Bloch modes  $p_q(r, \theta, t) = \sum_m P_{q,m} e^{i(m\kappa_r + \kappa)r} e^{i\omega t} e^{iq\theta}$  are shown in Figure 3d–o, whereby for better visualization the dependence from time is eliminated evaluating  $p_q(r, \theta, t)$  at  $t = 0$ . Different  $q$  values imply monopolar (Figure 3d,e,j,k), dipolar (Figure 3f,g,l,m), and quadrupolar (Figure 3h,i,n,o) associated symmetries and are labeled with roman numbers I–IV. It is straightforward to conclude that excitation with appropriate azimuthal symmetry are able to favor only the propagation of the corresponding Bloch modes (i.e., Bloch modes with different symmetries are orthogonal to the excitation). The modes obtained for  $q > 0$  display cutoff frequencies below which propagation is not allowed, which is typical of higher order modes in acoustic waveguides. In addition, a reciprocal gap, that occurs at the

same frequency for positive and negative wavenumbers, is present for any  $q$  values and is tailorable depending on the modulation parameters  $\alpha$  and  $\kappa_r$  [1].

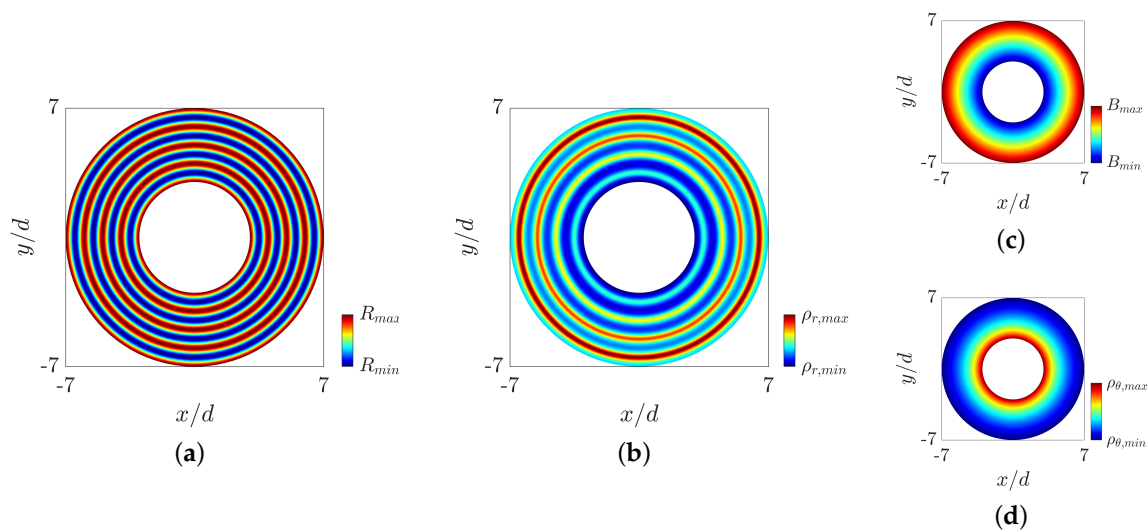


**Figure 2.** Schematic of the spatial modulation. (a) Graphical representation of  $R(r, \theta)$ . (b) Radial density distribution  $\rho_r(r, \theta)$  in space. (c) Representation of the bulk modulus  $B(r, \theta)$  in the plane. (d) Tangential density  $\rho_\theta(r, \theta)$  distribution in space.  $\rho_\theta(r, \theta)$  is inversely proportional to the radius, whereas  $B(r, \theta)$  is linearly increasing with  $r$ .

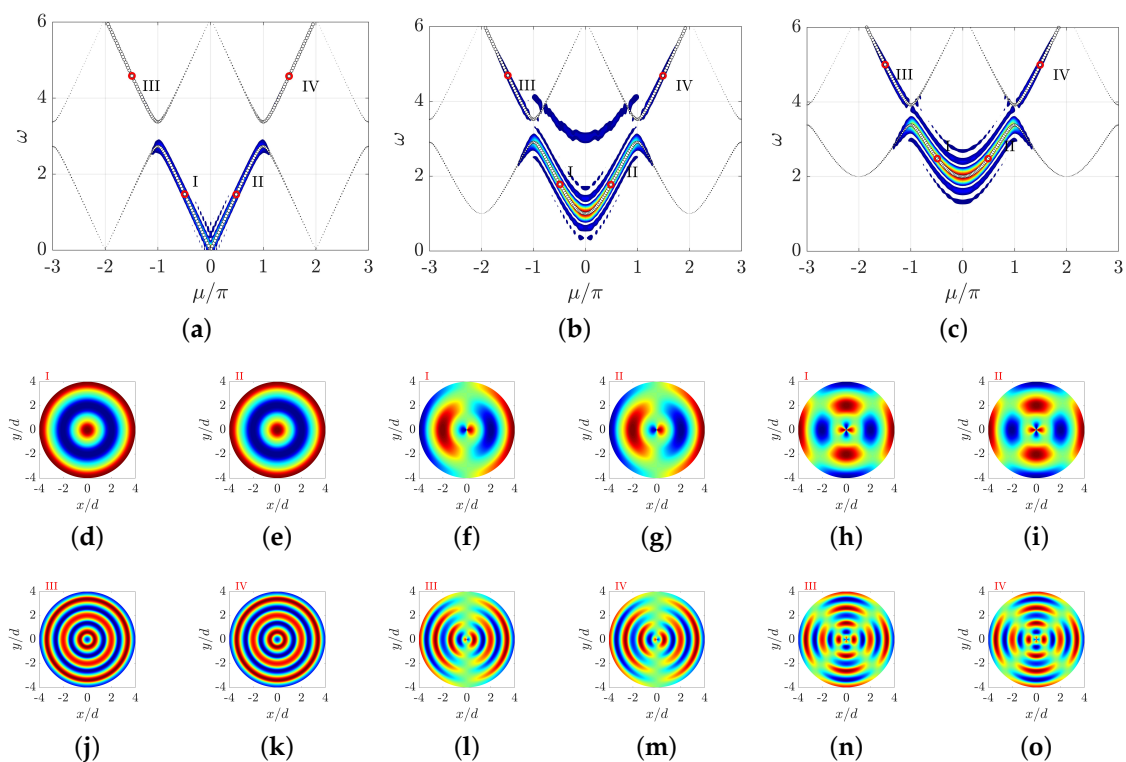


**Figure 3.** Numerical dispersion (colored contours) with superimposed Plane Wave Expansion Method (PWEM) solution (white dots) for (a)  $q = 0$ , (b)  $q = 1$ , (c) and  $q = 2$ . The Bloch-wave solutions corresponding to  $\mu/\pi = \pm 0.5$  and  $\mu/\pi = \pm 1.5$  are marked with red dots. The corresponding modes are illustrated below for (d,e,j,k)  $q = 0$ , (f,g,l,m)  $q = 1$ , and (h,i,n,o)  $q = 2$ .

The PWEM results are verified through numerical simulations with the Partial Differential Equation (PDE) interface provided by the COMSOL Multiphysics environment. The model solves the two dimensional wave equation with implemented spatiotemporal anisotropic material properties. Time domain analysis is performed within a finite RSC with inner and outer shells of diameter  $d_i = 1$  [m] and  $d_o = 45$  [m]. Wave propagation is excited with a broadband spectrum excitation in form of imposed acoustic velocity along the perimeter of the mean circumference, with appropriate azimuthal symmetry to excite each mode separately. The 2D FFT of the time history of the response along the radial direction is then performed to obtain the dispersion relation  $\hat{p}(\kappa, \omega)$  and superimposed for comparison in Figure 3a–c. The total time of simulation was set in order to avoid reflections at the inner and outer boundaries of the domain, these being set to be acoustically fixed.

### 3.2. Space–Time-Varying Radial Crystals

We now consider the modulation parameters used in the previous section for  $\alpha$  and  $\kappa_r$ , while a time periodicity for the radial density is enforced according to the following function:

$$R(r, t) = \cos(\kappa_r r - \omega_r t) = \sum_n R_n e^{in(\kappa_r r - \omega_r t)} \quad (12)$$

with  $\omega_r = 0.3\pi$ . The spatial distributions of the material properties and their evolution in time are depicted in Figure 4. Specifically,  $R(r, \theta, t) = R(r, t)$  is shown in Figure 4a and illustrates a modulation traveling from the outer to the inner shell, which implies a distribution of the radial density  $\rho_r(r, \theta, t) = \rho_r(r, t)$  as shown in Figure 4b. In contrast, the coefficients  $B_n = \Theta_n = \delta_{0n}$  imply time-invariant azimuthal density  $\rho_\theta(r, \theta, t) = \rho_\theta(r, t)$  and bulk modulus  $B(r, \theta, t) = B(r, t)$ , that are displayed in Figure 4c,d.

The dispersion properties for modes corresponding to  $q = 0, 1, 2$  are inspected through the PWEM in radial coordinates, and are shown in Figure 5. Compared to the space modulated media, a pair of directional bandgaps open in the  $\kappa - \omega$  space, as a blueprint of non reciprocity. This means that there are frequency bands in which diverging waves cannot propagate while incoming waves can, and vice-versa. Illustrative examples of counter-propagating Bloch modes  $p_q(r, \theta, t) = \sum_m P_{q,m} e^{i[(m\kappa_r + \kappa)r - (m\omega_r + \omega)t]} e^{i\theta}$  are shown below each dispersion (and labeled with roman numbers I–IV), corresponding to different azimuthal symmetries and therefore associated with the respective order  $q$ . The analytical predictions are checked employing time domain simulations with broadband frequency spectrum and the numerical dispersion is overlapped on the analytic one for comparison, showing good agreement. Moreover, the gap position and width are tailorable and can be set through a proper choice of the modulation parameters  $\alpha$ ,  $\kappa_r$ , and  $\omega_r$  according to the procedure described in [1].

Non-reciprocity is then further inspected through a narrowband excitation centered in correspondence of a directional bandgap and located in the central radius of the RSC. The time histories within the simulation interval  $t \in [0, T]$ , along with the recovered dispersion, are shown in Figure 6 for monopole, dipole, and quadrupole excitations. For simplicity, only the contribution along  $\theta = 45^\circ$  is displayed, whereby only diverging waves propagate thus confirming the one-way effects (see Supplementary Material for full animations of the time history).

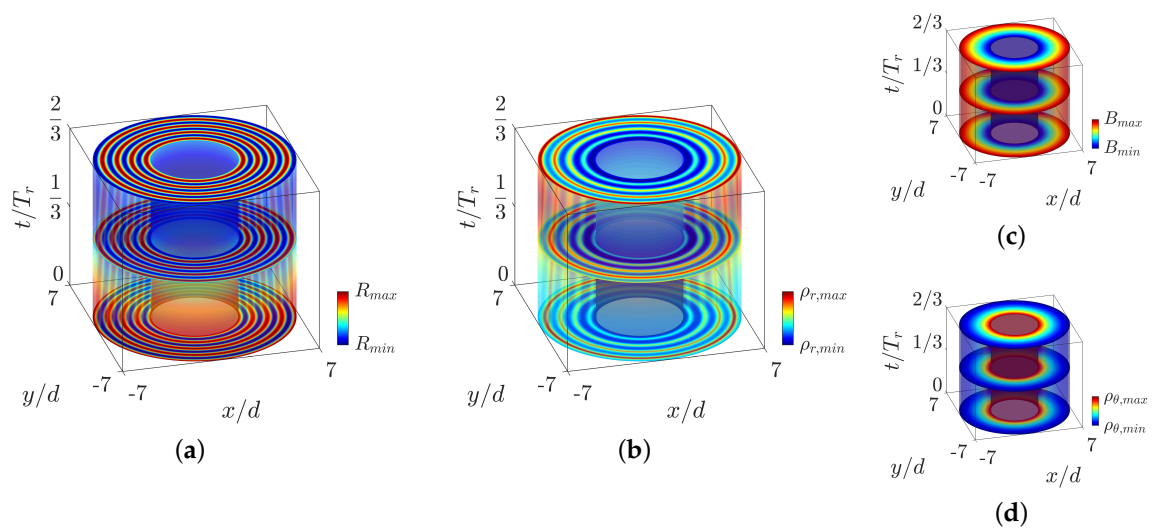


**Figure 4.** Schematic representation of the space–time varying properties. (a) Graphical representation of  $R(r, \theta, t)$ . (b) Space–time varying radial tension  $\rho_r(r, \theta, t)$ . The properties are periodic in space and traveling toward the inner shell or the outer shell depending on the modulation direction. (c) Bulk modulus distribution  $B(r, \theta, t)$ . (d) Graphical representation of the spatially varying tangential density  $\rho_\theta(r, \theta, t)$ .

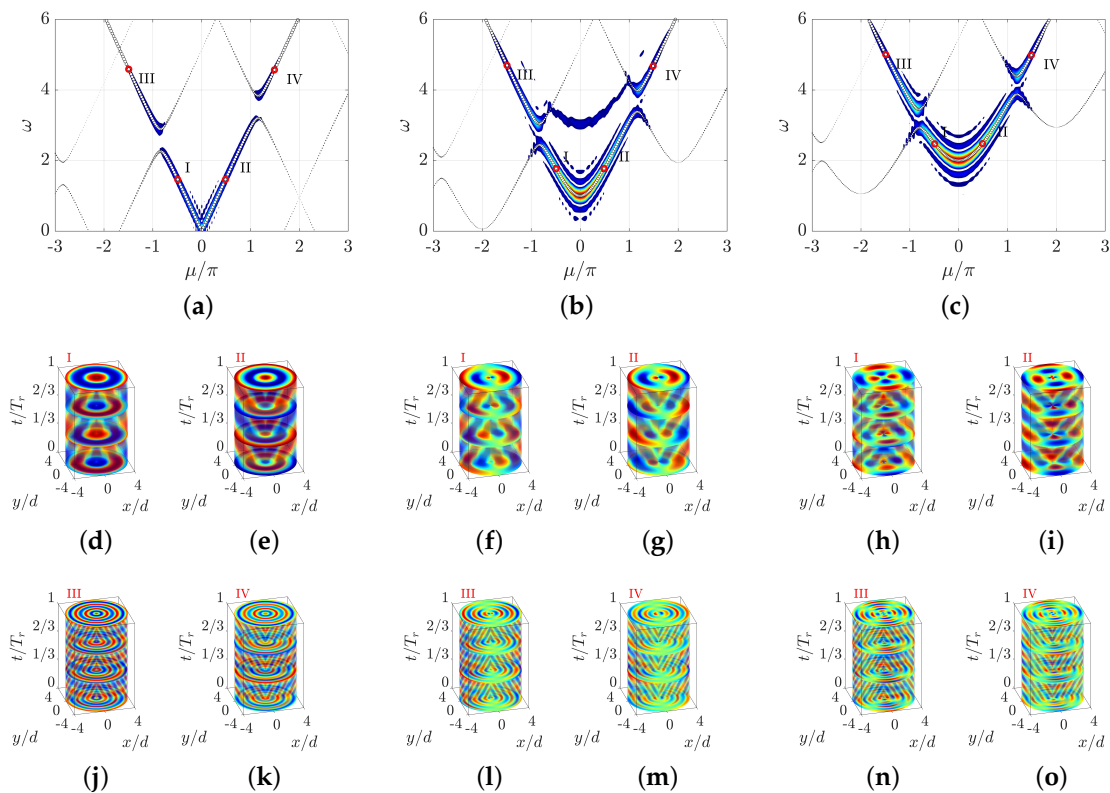


**Figure 5.** (a–c) Numerical dispersion relation (colored contours) for a space–time modulated SRC with superimposed PWEM solution (white dots). (a)  $q = 0$ ; (b)  $q = 1$ ; (c)  $q = 2$ . The Bloch-wave solutions corresponding to  $\mu/\pi = \pm 0.5$  and  $\mu/\pi = \pm 1.5$  are marked with red dots. The corresponding modes are illustrated below for (d,e,j,h)  $q = 0$ , (f,g,l,m)  $q = 1$ , and (h,i,n,o)  $q = 2$ .

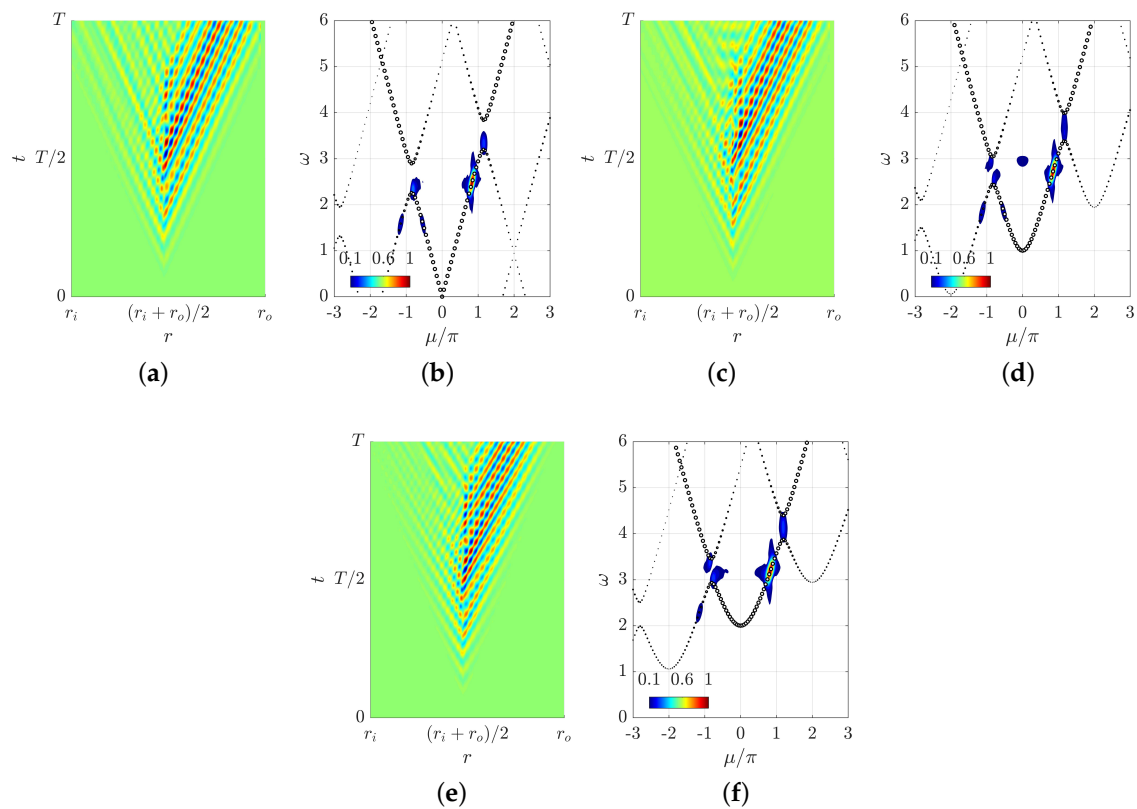


**Figure 6.** One-way wave propagation for a space–time modulated SRC with excitation in the middle of the ring structure and associated numerical and PWEM dispersion. **(a,b)** Monopole, **(c,d)** dipole, and **(e,f)** quadrupole excitation. The energy mainly propagates from the central portion to the outer shell, while propagation to the inner shell is not allowed.

#### 4. Discussion

In this paper we investigated spatiotemporally modulated radial sonic crystals. The evaluation of the wave propagation properties is carried out through the PWEM in polar coordinates, and then validated via numerical simulation of wave propagation and corresponding dispersion. We have shown that directional bandgaps can be induced for Bloch waves characterized by different azimuthal symmetries (monopolar, dipolar, and quadrupolar) and that omnidirectional one-way wave propagation is supported along the radial direction through a proper excitation mechanism.

This work paves the way for future studies on the practical realization of acoustic one-way emitters/receivers. The underlying hypothesis of the work is to be able to obtain tensorial dynamic densities modulated in time. Examples of metamaterials exhibiting equivalent tensorial densities are numerous and have been used extensively in the literature regarding metamaterials for controlling sound waves, for example in the context of transformation acoustics and cloaking ([27–30]). For what concerns active modulation of the equivalent properties, interesting studies have also been reported [31] both theoretically and experimentally [32–35]. A way of implementing anisotropy in a modulated acoustic medium has also been recently introduced by Allam et al. [36]. In conclusion, we also underline that the proposed approach is general and valid for all scalar wave systems upon appropriate substitutions of material properties as for example transverse vibrations in membranes, SH waves in bulk elastic materials, linear surface waves on water, and TM/TE modes in electromagnetism.

**Supplementary Materials:** The following are available online at <http://www.mdpi.com/2073-4352/10/7/624/s1>, Video S1: time history of monopole excitation, Video S2: time history of dipole excitation, Video S3: time history of quadrupole excitation.

**Author Contributions:** Conceptualization, D.E.Q.; methodology, D.E.Q.; software, D.E.Q., E.R.; validation, D.E.Q., E.R.; formal analysis, D.E.Q., E.R.; investigation, D.E.Q., E.R.; resources, D.E.Q., E.R.; data curation, D.E.Q., E.R.; writing—original draft preparation, D.E.Q., E.R.; writing—review and editing, D.E.Q., E.R., and G.C.; visualization, E.R.; supervision, G.C., F.B.; project administration, G.C., F.B.; funding acquisition, F.B. All authors have read and agreed to the published version of the manuscript.

**Funding:** This research received no external funding.

**Acknowledgments:** The Italian Ministry of Education, University and Research is acknowledged for the support provided through the Project “Department of Excellence LIS4.0—Lightweight and Smart Structures for Industry 4.0.

**Conflicts of Interest:** The authors declare no conflict of interest. The funders had no role in the design of the study; in the collection, analyses, or interpretation of data; in the writing of the manuscript, or in the decision to publish the results.

## Abbreviations

The following abbreviations are used in this manuscript:

PWEM Plane Wave Expansion Method

RSC Radial Sonic Crystal

## Appendix A. PWEM for a Spatially Modulated RSC

Consider the wave equation:

$$\left[ -\frac{B(r)}{r} \frac{\partial}{\partial r} \frac{r}{\rho_r(r)} \frac{\partial}{\partial r} + q^2 \frac{B(r)}{r^2 \rho_\theta(r)} \right] P_q(r) = \omega^2 P_q(r) \quad (\text{A1})$$

The material densities  $\rho_r(r, \theta)$  and  $\rho_\theta(r, \theta)$  and bulk modulus  $B(r, \theta)$  are expanded as:

$$\begin{aligned} B(r) &= r \sum_n B_n e^{in\kappa_r r} \\ \frac{1}{\rho_r(r)} &= \frac{\sum_n R_n e^{in\kappa_r r}}{r} \\ \frac{1}{\rho_\theta(r)} &= r \sum_n \Theta_n e^{in\kappa_r r} \end{aligned} \quad (\text{A2})$$

where  $\kappa_r = 2\pi/d$  is the modulation wavenumber and  $d$  is the spatial period. Consider an Ansatz solution in form of a Bloch wave:

$$p_q(r) = \sum_m P_{q,m} e^{i(m\kappa_r + \kappa)r} \quad (\text{A3})$$

substituting Equations (A2) and (A3) in the governing Equation (A1) gives:

$$\left[ -\sum_s B_s e^{is\kappa_r r} \frac{\partial}{\partial r} \sum_n R_n e^{in\kappa_r r} \frac{\partial}{\partial r} + q^2 \sum_{s,l} B_s \Theta_l e^{i(s+l)\kappa_r r} \right] \sum_m P_{q,m} e^{i(m\kappa_r + \kappa)r} = \omega^2 \sum_m P_{q,m} e^{i(m\kappa_r + \kappa)r} \quad (\text{A4})$$

thus

$$-\sum_s B_s e^{is\kappa_r r} \frac{\partial}{\partial r} \sum_{n,m} i(m\kappa_r + \kappa) P_{q,m} R_n e^{i[(n+m)\kappa_r + \kappa]r} + q^2 \sum_{s,l,m} B_s \Theta_l P_{q,m} e^{i[(s+l+m)\kappa_r + \kappa]r} = \omega^2 \sum_m P_{q,m} e^{i(m\kappa_r + \kappa)r} \quad (\text{A5})$$

multiplying both side by  $e^{is\kappa_r r}$

$$\sum_{s,n,m} (m\kappa_r + \kappa)[(n+m)\kappa_r + \kappa] B_s P_{q,m} R_n e^{i(n+m+s)\kappa_r r} + q^2 \sum_{s,l,m} B_s \Theta_l P_{q,m} e^{i(s+l+m)\kappa_r r} = \omega^2 \sum_m P_{q,m} e^{im\kappa_r r} \quad (\text{A6})$$

enforcing the orthogonality of exponential functions we get to:

$$\sum_{n,m} (m\kappa_r + \kappa)[(n + m)\kappa_r + \kappa] B_{w-n-m} P_{q,m} R_n + q^2 \sum_{l,m} B_{w-l-m} \Theta_l P_{q,m} = \omega^2 P_{q,w} \tag{A7}$$

this can be recasted in an eigenvalue problem in the form

$$[H(\kappa)] \mathbf{P}_q = \omega^2 \mathbf{P}_q \tag{A8}$$

for example consider  $-1 \leq n, m, l, w \leq 1$  then

$$\mathbf{P}_q = \begin{bmatrix} P_{q,-1} \\ P_{q,0} \\ P_{q,1} \end{bmatrix} \tag{A9}$$

and

$$[H(\kappa)] = \sum_n [L_n(\kappa)] + \sum_l [Q_l] \tag{A10}$$

with

$$\begin{aligned} [L_n(\kappa)]_{ij} &= (j\kappa_r + \kappa)[(n + j)\kappa_r + \kappa] B_{i-n-j} R_n \quad -1 < i, j < 1 \\ [Q_l]_{ij} &= q^2 B_{i-l-j} \Theta_l \quad -1 < i, j < 1 \end{aligned} \tag{A11}$$

### Appendix B. PWEM for a Spatiotemporally Modulated RSC

Consider now space-time periodic material parameters, which can be suitably expanded as follows:

$$\begin{aligned} B(r, t) &= r \sum_n B_n e^{in\kappa_r r - \omega_r t} \\ \frac{1}{\rho_r(r, t)} &= \frac{\sum_n R_n e^{in\kappa_r r - \omega_r t}}{r} \\ \frac{1}{\rho_\theta(r, t)} &= r \sum_n \Theta_n e^{in\kappa_r r - \omega_r t} \end{aligned} \tag{A12}$$

where  $\omega_r = 2\pi/T_r$  is the temporal angular frequency and  $T_r$  is the temporal period. The Ansatz solution possess the same periodicity of the material parameters:

$$p_q(r) = \sum_m P_{q,m} e^{i[(m\kappa_r + \kappa)r - (m\omega_r + \omega)t]} \tag{A13}$$

substituting the expressions in Equations (A12) and (A13) the in the governing equation of motion:

$$\left[ -\sum_s B_s e^{is(\kappa_r r - \omega_r t)} \frac{\partial}{\partial r} \sum_n R_n e^{in(\kappa_r r - \omega_r t)} \frac{\partial}{\partial r} + q^2 \sum_{s,l} B_s \Theta_l e^{i(s+l)(\kappa_r r - \omega_r t)} \right] \sum_m P_{q,m} e^{i[(m\kappa_r + \kappa)r - (m\omega_r + \omega)t]} = \sum_m (m\omega_m + \omega)^2 P_{q,m} e^{i[(m\kappa_r + \kappa)r - (m\omega_r + \omega)t]} \tag{A14}$$

which can be re-written as:

$$\begin{aligned} & -\sum_s B_s e^{is(\kappa_r r - \omega_r t)} \frac{\partial}{\partial r} \sum_{n,m} i(m\kappa_r + \kappa) P_{q,m} R_n e^{i\{[(n+m)\kappa_r + \kappa]r - [(n+m)\omega_r + \omega]t\}} + \\ & + q^2 \sum_{s,l,m} B_s \Theta_l P_{q,m} e^{i\{(s+l+m)\kappa_r + \kappa\}r - \{(s+l+m)\omega_r + \omega\}t} = \sum_m (m\omega_r + \omega)^2 P_{q,m} e^{i[(m\kappa_r + \kappa)r - (m\omega_r + \omega)t]} \end{aligned} \tag{A15}$$

the multiplication by  $e^{is(\kappa_r r - \omega_r t)}$  yields:

$$\begin{aligned} & \sum_{s,n,m} (m\kappa_r + \kappa)[(n+m)\kappa_r + \kappa] B_s P_{q,m} R_n e^{i(n+m+s)(\kappa_r r - \omega_r t)} + \\ & + q^2 \sum_{s,l,m} B_s \Theta_l P_{q,m} e^{i(s+l+m)(\kappa_r r - \omega_r t)} = \sum_m (m\omega_r + \omega)^2 P_{q,m} e^{im(\kappa_r r - \omega_r t)} \end{aligned} \quad (\text{A16})$$

exploiting the orthogonality of the exponential function we get to:

$$\sum_{n,m} (m\kappa_r + \kappa)[(n+m)\kappa_r + \kappa] B_{w-m-n} P_{q,m} R_n + q^2 \sum_{l,m} B_{w-l-m} \Theta_l P_{q,m} = (w\omega_r + \omega)^2 P_{q,w} \quad (\text{A17})$$

which can be written as a quadratic eigenvalue problem (QEP)

$$\omega_r^2 [M_2] + \omega [M_1] + [M_0(\kappa)] = 0 \quad (\text{A18})$$

where:

$$\begin{aligned} [M_2] &= [I] \\ [M_1]_{ij} &= 2\omega_r i \delta_{ij} \\ [M_0]_{ij} &= \omega_r^2 i^2 \delta_{ij} - [H(k)]_{ij} \end{aligned} \quad (\text{A19})$$

## References

1. Trainiti, G.; Ruzzene, M. Non-reciprocal elastic wave propagation in spatiotemporal periodic structures. *New J. Phys.* **2016**, *18*, 083047. [\[CrossRef\]](#)
2. Vila, J.; Pal, R.K.; Ruzzene, M.; Trainiti, G. A bloch-based procedure for dispersion analysis of lattices with periodic time-varying properties. *J. Sound Vib.* **2017**, *406*, 363–377. [\[CrossRef\]](#)
3. Riva, E.; Marconi, J.; Cazzulani, G.; Braghin, F. Generalized plane wave expansion method for non-reciprocal discretely modulated waveguides. *J. Sound Vib.* **2019**, *449*, 172–181. [\[CrossRef\]](#)
4. Nassar, H.; Chen, H.; Norris, A.; Haberman, M.; Huang, G. Non-reciprocal wave propagation in modulated elastic metamaterials. *Proc. R. Soc. A Math. Phys. Eng. Sci.* **2017**, *473*, 20170188. [\[CrossRef\]](#)
5. Marconi, J.; Cazzulani, G.; Riva, E.; Braghin, F. Observations on the behavior of discretely modulated spatiotemporal periodic structures. In *Active and Passive Smart Structures and Integrated Systems XII*; International Society for Optics and Photonics: Bellingham, WA USA, 2018; Volume 10595, p. 105952N.
6. Riva, E.; Quadrelli, D.E.; Marconi, J.; Cazzulani, G.; Braghin, F. Design and experimental analysis of nonreciprocal wave propagation in a space-time modulated beam. In *Active and Passive Smart Structures and Integrated Systems IX*; International Society for Optics and Photonics: Bellingham, WA USA, 2020; Volume 11376, p. 1137613.
7. Li, J.; Shen, C.; Zhu, X.; Xie, Y.; Cummer, S.A. Nonreciprocal sound propagation in space-time modulated media. *Phys. Rev. B* **2019**, *99*, 144311. [\[CrossRef\]](#)
8. Karkar, S.; De Bono, E.; Collet, M.; Matten, G.; Ouisse, M.; Rivet, E. Broadband Nonreciprocal Acoustic Propagation Using Programmable Boundary Conditions: From Analytical Modeling to Experimental Implementation. *Phys. Rev. Appl.* **2019**, *12*, 054033. [\[CrossRef\]](#)
9. Fleury, R.; Sounas, D.L.; Alù, A. Subwavelength ultrasonic circulator based on spatiotemporal modulation. *Phys. Rev. B* **2015**, *91*, 174306. [\[CrossRef\]](#)
10. Chamanara, N.; Taravati, S.; Deck-Léger, Z.L.; Caloz, C. Optical isolation based on space-time engineered asymmetric photonic band gaps. *Phys. Rev. B* **2017**, *96*, 155409. [\[CrossRef\]](#)
11. Marconi, J.; Riva, E.; Di Ronco, M.; Cazzulani, G.; Braghin, F.; Ruzzene, M. Experimental Observation of Nonreciprocal Band Gaps in a Space-Time-Modulated Beam Using a Shunted Piezoelectric Array. *Phys. Rev. Appl.* **2020**, *13*, 031001. [\[CrossRef\]](#)
12. Riva, E.; Casieri, V.; Resta, F.; Braghin, F. Adiabatic pumping via avoided crossings in stiffness modulated quasiperiodic beams. *arXiv* **2020**, arXiv:2003.11525.

13. Attarzadeh, M.; Callanan, J.; Nouh, M. Experimental observation of nonreciprocal waves in a resonant metamaterial beam. *Phys. Rev. Appl.* **2020**, *13*, 021001. [[CrossRef](#)]
14. Attarzadeh, M.; Maleki, S.; Crassidis, J.; Nouh, M. Non-reciprocal wave phenomena in energy self-reliant gyric metamaterials. *J. Acoust. Soc. Am.* **2019**, *146*, 789–801. [[CrossRef](#)] [[PubMed](#)]
15. Chen, Y.; Li, X.; Nassar, H.; Norris, A.N.; Daraio, C.; Huang, G. Nonreciprocal wave propagation in a continuum-based metamaterial with space-time modulated resonators. *Phys. Rev. Appl.* **2019**, *11*, 064052. [[CrossRef](#)]
16. Shen, C.; Li, J.; Jia, Z.; Xie, Y.; Cummer, S.A. Nonreciprocal acoustic transmission in cascaded resonators via spatiotemporal modulation. *Phys. Rev. B* **2019**, *99*, 134306. [[CrossRef](#)]
17. Li, J.; Zhu, X.; Shen, C.; Peng, X.; Cummer, S.A. Transfer matrix method for the analysis of space-time-modulated media and systems. *Phys. Rev. B* **2019**, *100*, 144311. [[CrossRef](#)]
18. Cummer, S.A.; Christensen, J.; Alù, A. Controlling sound with acoustic metamaterials. *Nat. Rev. Mater.* **2016**, *1*, 16001. [[CrossRef](#)]
19. Zangeneh-Nejad, F.; Fleury, R. Active times for acoustic metamaterials. *Rev. Phys.* **2019**, *4*, 100031. [[CrossRef](#)]
20. Deck-Léger, Z.L.; Chamanara, N.; Skorobogatiy, M.; Silveirinha, M.G.; Caloz, C. Uniform-velocity spacetime crystals. *Adv. Photonics* **2019**, *1*, 056002. [[CrossRef](#)]
21. Taravati, S.; Chamanara, N.; Caloz, C. Nonreciprocal electromagnetic scattering from a periodically space-time modulated slab and application to a quasisonic isolator. *Phys. Rev. B* **2017**, *96*, 165144. [[CrossRef](#)]
22. Cassedy, E.; Oliner, A. Dispersion relations in time-space periodic media: Part I—Stable interactions. *Proc. IEEE* **1963**, *51*, 1342–1359. [[CrossRef](#)]
23. Cassedy, E. Dispersion relations in time-space periodic media part II—Unstable interactions. *Proc. IEEE* **1967**, *55*, 1154–1168. [[CrossRef](#)]
24. Attarzadeh, M.; Nouh, M. Non-reciprocal elastic wave propagation in 2D phononic membranes with spatiotemporally varying material properties. *J. Sound Vib.* **2018**, *422*, 264–277. [[CrossRef](#)]
25. Riva, E.; Di Ronco, M.; Elabd, A.; Cazzulani, G.; Braghin, F. Non-reciprocal wave propagation in discretely modulated spatiotemporal plates. *J. Sound Vib.* **2020**, *471*, 115186. [[CrossRef](#)]
26. Torrent, D.; Sánchez-Dehesa, J. Radial Wave Crystals: Radially Periodic Structures from Anisotropic Metamaterials for Engineering Acoustic or Electromagnetic Waves. *Phys. Rev. Lett.* **2009**, *103*, 064301. [[CrossRef](#)]
27. Zigoneanu, L.; Popa, B.I.; Starr, A.F.; Cummer, S.A. Design and measurements of a broadband two-dimensional acoustic metamaterial with anisotropic effective mass density. *J. Appl. Phys.* **2011**, *109*, 054906. [[CrossRef](#)]
28. Zigoneanu, L.; Popa, B.I.; Cummer, S.A. Three-dimensional broadband omnidirectional acoustic ground cloak. *Nat. Mater.* **2014**, *13*, 352–355. [[CrossRef](#)] [[PubMed](#)]
29. Pendry, J.; Li, J. An acoustic metafluid: Realizing a broadband acoustic cloak. *New J. Phys.* **2008**, *10*, 115032. [[CrossRef](#)]
30. Torrent, D.; Sánchez-Dehesa, J. Anisotropic mass density by two-dimensional acoustic metamaterials. *New J. Phys.* **2008**, *10*, 023004. [[CrossRef](#)]
31. Chen, S.; Fan, Y.; Fu, Q.; Wu, H.; Jin, Y.; Zheng, J.; Zhang, F. A review of tunable acoustic metamaterials. *Appl. Sci.* **2018**, *8*, 1480. [[CrossRef](#)]
32. Baz, A.M. An active acoustic metamaterial with tunable effective density. *J. Vib. Acoust.* **2010**, *132*. [[CrossRef](#)]
33. Akl, W.; Baz, A. Experimental characterization of active acoustic metamaterial cell with controllable dynamic density. *J. Appl. Phys.* **2012**, *112*, 084912. [[CrossRef](#)]
34. Allam, A.; Elabbagh, A.; Akl, W. Experimental demonstration of one-dimensional active plate-type acoustic metamaterial with adaptive programmable density. *J. Appl. Phys.* **2017**, *121*, 125106. [[CrossRef](#)]
35. Popa, B.I.; Zigoneanu, L.; Cummer, S.A. Tunable active acoustic metamaterials. *Phys. Rev. B* **2013**, *88*, 024303. [[CrossRef](#)]
36. Allam, A.; Elabbagh, A.; Akl, W. Modeling and design of two-dimensional membrane-type active acoustic metamaterials with tunable anisotropic density. *J. Acoust. Soc. Am.* **2016**, *140*, 3607–3618. [[CrossRef](#)] [[PubMed](#)]

